Evidence of deuterium excess in water vapor as an indicator of ocean surface conditions

JOURNAL OF GEOPHYSICAL RESEARCH, VOL. 113, D19114, doi:10.1029/2008JD010209, 2008

Evidence of deuterium excess in water vapor as an indicator of ocean surface conditions

Ryu Uemura,[1,2] Yohei Matsui,[3,4] Kei Yoshimura,[5] Hideaki Motoyama,[1] and Naohiro Yoshida[3]

Received 2 April 2008; revised 10 July 2008; accepted 23 July 2008; published 14 October 2008.

[1] Stable isotopes of water are important climatic tracers used to understand atmospheric moisture cycling and to reconstruct paleoclimate. The combined use of hydrogen and oxygen isotopes in water provides an additional parameter, deuterium excess (d), which might reflect ocean surface conditions in moisture source regions for precipitation. The d records from polar ice cores covering glacial-interglacial cycles were used to reconstruct ocean surface temperatures at the moisture source, enabling elimination of source effects from the conventional isotope thermometer. However, observations of the essential relationship between d in vapor and ocean surface conditions are very limited. To date, theoretical values predicted using simple and atmospheric general circulation models (GCM) have not been validated against the data. Here, we show the isotope ratios of atmospheric water vapor near the ocean surface in middle and high latitudes of the Southern Ocean. Our observations show that d negatively correlates with relative humidity (h) above the ocean and correlates with sea surface temperature (SST). Despite the fact that the GCMs would underestimate the absolute value of observed d, the observations and simulation results are consistent for slopes between d versus h and d versus SST, suggesting that d is a reliable index to h and SST over the ocean surface.

Citation: Uemura, R., Y. Matsui, K. Yoshimura, H. Motoyama, and N. Yoshida (2008), Evidence of deuterium excess in water vapor as an indicator of ocean surface conditions, *J. Geophys. Res.*, *113*, D19114, doi:10.1029/2008JD010209.

1. Introduction

[2] The stable isotope ratios of hydrogen (D/H) and oxygen ($^{18}O/^{16}O$) in water reflect various exchanges between water phases through the global water cycle. These isotope ratios are important climatic tracers used to understand atmospheric moisture cycling [*Worden et al.*, 2007; *Yamanaka and Shimizu*, 2007; *Noone*, 2008] and to reconstruct paleoclimate from ice cores [*EPICA Community Members*, 2004; *Kawamura et al.*, 2007]. The relative abundance of the heavy isotopes, $HD^{16}O$ and $H_2^{18}O$, is represented by the delta value, $\delta = (R_{sa}/R_{VSMOW} - 1)$, where R_{sa} is the isotope ratio of sample and R_{VSMOW} is the isotope ratio of the Vienna Standard Mean Ocean Water (VSMOW). Past air temperatures can be inferred by either δD or $\delta^{18}O$ in the ice core because the equilibrium fractionation between vapor and condensate is temperature-dependent. In addition, the precipitation moisture source information can be derived from the deuterium excess ($d = \delta D - 8 \times \delta^{18}O$) parameter, which mainly reflects the kinetic fractionation process, such as evaporation from the ocean into the atmosphere [*Dansgaard*, 1964].

[3] Evaporation, as the first step in the hydrological cycle, plays a key role in determining relation between δD and $\delta^{18}O$ in global precipitation and snow. A Craig-Gordon type simple evaporation model [*Craig and Gordon*, 1965; *He and Smith*, 1999] describes the initial isotope content in the water vapor (δ_{v0}) as a function of the isotope contents of the evaporating water (δ_E), deuterium excess (d), relative humidity (h), and sea surface temperature (SST). Note that relative humidity is defined as a value normalized on the SST (h^*) in the model. The value of h^* can be approximated to h near the ocean surface because the SST is almost equivalent to the air temperature.

[4] However, the value of δ_{v0} is not estimated easily because it is difficult to estimate or observe the δ_E. Making a global-scale closure assumption ($\delta_{v0} = \delta_E$) [*Merlivat and Jouzel*, 1979], the model can be written as

$$1 + \delta_{V0} = \frac{1}{\alpha}\frac{(1-k)}{1-kh}(1 + \delta_{\mathrm{ocean}}), \qquad (1)$$

where k is a kinetic fractionation factor, α is an equilibrium fractionation factor, and δ_{ocean} is an ocean isotope composition. In principle, the d versus h correlation arises because the magnitude of the kinetic effect (i.e., moisture

[1]National Institute of Polar Research, Research Organization of Information and Systems, Tokyo, Japan.
[2]Now at Laboratoire des Sciences du Climat et l'Environnement, CEA-CNRS, Gif-sur-Yvette, France.
[3]Department of Environmental Science and Technology, Tokyo Institute of Technology, Tokyo, Japan.
[4]Now at School of Earth Sciences, Ohio State University, Columbus, Ohio, USA.
[5]Climate Research Division, Scripps Institution of Oceanography, La Jolla, California, USA.

0148-0227/08/2008JD010209$09.00

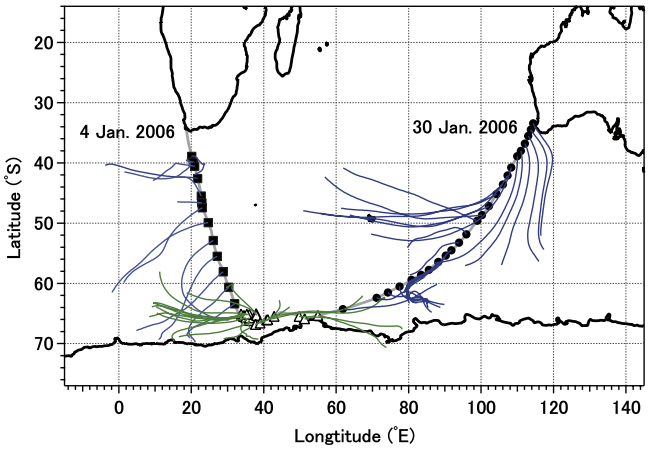

Figure 1. Sampling sites on a map of the ship route (gray) and 2 day backward trajectories (from 35 to 65°S shown by the blue line and south of 65°S shown by the green line) and each sampling site (solid squares, open triangles, and solid circles).

gradient between sea surface and overlying unsaturated vapor) governs molecular diffusive transport from the saturated layer to drier free air. On the other hand, the d is also controlled by the SST through the temperature dependence of α. This model predicts that d in marine vapor increases when relative humidity (h) decreases (−0.43‰/%) and when the sea surface temperature (SST) increases (0.35‰/°C) [*Merlivat and Jouzel*, 1979]. Although this estimation is useful to understand underlying mechanism between d and ocean surface conditions, the global-scale closure assumption ($\delta_{v0} = \delta_E$) causes systematic bias [*Jouzel and Koster*, 1996]. A thorough method to predict the isotope ratios of marine vapor is to simulate the water cycle using an atmospheric general circulation models (GCMs) that accounts for complexity of hydrological processes [*Joussaume et al.*, 1984; *Jouzel et al.*, 1987; *Hoffmann et al.*, 1998; *Mathieu et al.*, 2002].

[5] The subsequent precipitation process, which is controlled by equilibrium fractionation, would exert a minor impact on the d parameter; thereby, changes in ocean surface conditions at the moisture source can be estimated from the d in polar precipitation. The d records from Antarctic ice cores show that significant ∼41,000 year periodicity cycle over the glacial-interglacial cycles [*Vimeux et al.*, 1999; *Vimeux et al.*, 2001; *Uemura et al.*, 2004]. Because d depends on SST, h, and the wind speed at the vapor source region and on the supersaturation ratio where snow crystals form [*Jouzel and Merlivat*, 1984], several assumptions are necessary to interpret d in ice cores as an index of a single variable. The glacial-interglacial changes in d were interpreted as changes in relative humidity [*Jouzel et al.*, 1982] and temperatures at the moisture source ocean [*Cuffey and Vimeux*, 2001; *Stenni et al.*, 2001; *Vimeux et al.*, 2002]. In particular, information related to the moisture source temperature is valuable for accurate estimation of past air temperature changes at the site [*Cuffey and Vimeux*, 2001; *Masson-Delmotte et al.*, 2005].

[6] However, the interpretation of d in ice cores relies on the fact that various models, which range from simple Rayleigh-type models [*Jouzel and Merlivat*, 1984; *Johnsen et al.*, 1989; *Ciais and Jouzel*, 1994] to the isotopic general circulation model (GCM), predict a close relationship between d and ocean surface conditions. The crucial relationship between d, SST and h has not yet been validated against data related to the initial vapor because of scarce observations on d of vapor near the ocean surface and its physical conditions. A few in situ measurements of vapor isotopes in the oceans have been reported [*Craig and Gordon*, 1965; *Lawrence et al.*, 2004]; most of them specifically pertain to either δD or δ^{18}O. In fact, d has not been observed except for subtropical oceans [*Craig and Gordon*, 1965] and the Mediterranean Sea [*Gat and Garmi*, 1970; *Gat et al.*, 2003]. To fill the data gap on the vapor isotope compositions in the Southern Ocean, we measured isotope compositions of air moisture using a mechanical cold trap on a ship over the South Indian Ocean and Southern Ocean, which is a part of main moisture source (30°S – 65°S ocean) for Antarctic precipitation [*Delaygue et al.*, 2000] (Figure 1). Our observations show that d negatively correlates with relative humidity (h) above the ocean and correlates with sea surface temperature (SST). We discuss the differences between the observation and simulation results from a couple of isotope GCMs; a rather conventional simulation forced only by surface boundary (SST and sea ice) [*Jouzel et al.*, 1987; *Delaygue et al.*, 2000] and a more realistic simulation in high time resolution from a newly developed isotope GCM with additional forcing of observed atmospheric thermodynamical fields [*Yoshimura et al.*, 2008].

2. Methods

2.1. Performance Test of Vapor Sampler

[7] Atmospheric vapor was sampled cryogenically using a specially designed glass flask for determination of isotope ratios. Since accurate and precise sampling of vapor is needed in order to investigate d parameter, we carefully developed a vapor sampling system and tested its performance. Figure 2 shows a glass-made water vapor sampler that is designed for widely ranged vapor concentrations. This trap is an adaptation of Horibe trap [*Horibe and*

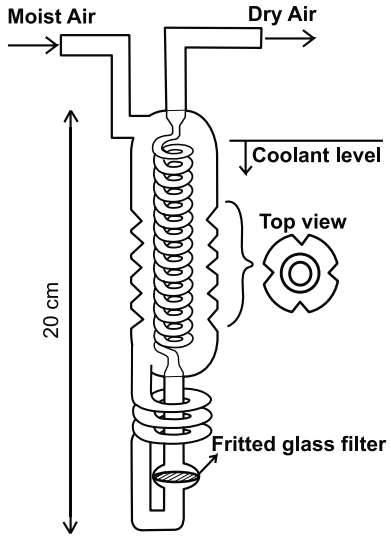

Figure 2. Schematic of glass made vapor trap.

Table 1. Efficiency Test for Vapor Trapping Apparatus

	Melted Iceberg		Distilled Sea Water	
	Trapped Vapor (n = 5)[a]	Injected Water (n = 10)[b]	Trapped Vapor (n = 2)[a]	Injected Water (n = 4)[b]
δD (‰)	−283.4 ± 0.5	−284.5 ± 0.3	−1.0 ± 0.9	−1.2 ± 0.2
δ^{18}O (‰)	−36.41 ± 0.04	−36.54 ± 0.02	−0.37 ± 0.08	−0.37 ± 0.0
d (‰)	7.8 ± 0.4	7.8	2.0 ± 1.6	1.8

[a]Average and standard deviation (1σ) of the replicated experiments (n indicates number of experiments).
[b]Average and standard deviation of the replicated experiments (n indicates number of measurements of water against VSMOW and Standard Light Antarctic Precipitation waters).

Takakuwa, 1973]. Residual vapor were sufficiently trapped by narrow and long glass tube, and a glass filter prevents outflow of trapped snow. The major modification is that spiral tube was inserted inside of wide end (∼45 mm OD) where the vapor is trapped efficiently with the surface of spiral tube cooled by the dry air. Further, the trap is compact enough to use onboard ship.

[8] The accuracy of the vapor sampling system had been tested carefully in the laboratory. The apparatus developed for the test comprises (1) a drying air unit, (2) a water injection port, and (3) a cold trap. All components were connected with a Teflon tube (fluorocarbon polymer, 3/8 inch) and Cajon and Swagelok (Swagelok Co., Ohio, USA) connections. First, the water vapor in the laboratory air was removed using a drying unit containing silica gel and a glass-made cold trap that was placed in a Dewar flask filled with liquid nitrogen. Second, the line led to a glass tube with a septum port from which water was injected. To enhance evaporation, a part of tubing was narrowed so that water bubbled within the tube. Then, the generated vapor was trapped cryogenically using a vapor trap in dry ice fluorinert bath with temperature maintained between −75 and −78°C (The flourinert is a liquid fluoric compound that has very low viscosity at low temperatures).

[9] After the tube and cold trap had been sufficiently dried by the dried air, 3.00 g of the water was injected into the septum. Humidity and temperature of the evolved moist air were monitored using a sensor situated within the line. Approximately 3 h after injection, all water was evaporated during which the relative humidity of moist air was changed from ∼95 to ∼0%. Both ends of cold trap were sealed immediately with Parafilm. The Parafilm was used to avoid the risk of bursting of the glass trap from expansion of the air. After the trapped vapor (ice and snow) was melted, the ends were plugged immediately with silicon stoppers. The weight of the cold trap was measured before and after the collection; the calculated weight recovery was 100 ± 0.01%, suggesting that the fraction of lost vapor is very small. Two water samples, a melted iceberg and distilled seawater, were used for the test; the results are presented in Table 1. Deviations between the sampled and known waters were 1‰ for δD and 0.05‰ for δ^{18}O. Although the isotope ratios of the collected vapor were slightly heavier than those of the original waters, these values are mutually indistinguishable in 2-sigma of analytical error.

2.2. Ship Observation and Isotope Analysis

[10] Observations were conducted between 30 December 2005 to 30 January 2006 along the route linking Cape Town, Lützow-Holm Bay, and Fremantle onboard the Tokyo Kaiyou Daigaku *R/V* Umitaka-maru during the 18th Cruise (Figure 1). Isotopic sampling was done 2–3 times per day (sampling time is ∼2–12 h), which corresponds to ∼10–400 km on a spatial scale. Air temperature and relative humidity were measured at 15 m altitude on the ship. Unfortunately, reliable data of wind speed at the sampling height was not available.

[11] Figure 3 shows a vapor sampling system that was installed in the bridge deck, in the wheelhouse. The inlet of the air-sampling device, which was covered using a droplet-shielding filter, was installed on the ship at 15 m altitude. We add a bypass line to avoid ship exhaust gas contamination. The solenoid valves, which are controlled by an anemometer, were changed automatically so that the polluted air from

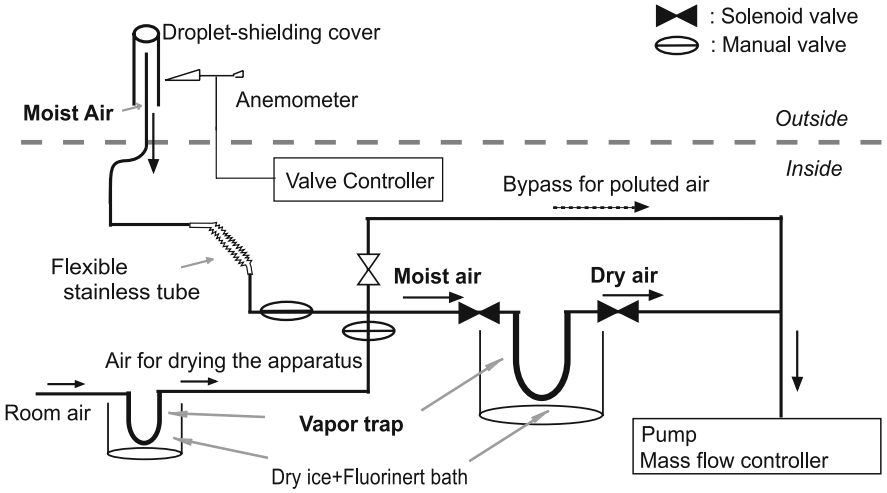

Figure 3. Schematic of the sampling system installed on the ship.

Table 2. Isotope Ratios in Water Vapor and Meteorological Conditions Along With the Ship Route

Sampling Start Time (UTC)	Sampling Duration (h)	Latitude[a] (°S)	Longtitude[a] (°E)	Atmospheric Pressure (hPa)	Air Temperature (°C)	SST(°C)	h(%)	Vapor Isotopes δ^{18}O(‰)	Vapor Isotopes δD(‰)	Vapor Isotopes d(‰)
Leg 1 (Cape Town to Antarctica)										
5 Jan. 0413	0142	38.91	20.11	1017	18.3	22.8	63.7	−15.71	−91.7	34.0
5 Jan. 0845	0300	39.86	20.53	1018	19.4	21.5	57.0	−14.56	−86.5	30.0
5 Jan. 1310	0308	40.56	20.93	1016	18.7	21.2	65.8	−14.47	−96.3	19.5
5 Jan. 1757	1056	42.59	21.75	1012	13.0	11.6	86.3	−12.09	−90.1	6.6
6 Jan. 0748	0802	45.49	22.73	989	10.8	8.2	89.3	−12.36	−96.4	2.5
6 Jan. 1740	1116	46.65	22.94	984	4.7	5.7	81.1	−15.86	−116.3	10.6
7 Jan. 0820	0440	47.45	23.05	1001	4.9	5.8	69.8	−15.93	−117.1	10.3
7 Jan. 1610	1233	49.92	24.65	999	2.4	3.7	80.1	−15.42	−115.6	7.7
8 Jan. 0810	0735	52.88	26.04	998	1.7	1.6	82.3	−13.90	−110.5	0.7
8 Jan. 1840	1020	55.51	27.17	999	0.9	1.7	71.8	−17.73	−131.6	10.2
9 Jan. 0805	0715	58.09	28.83	995	0.9	1.3	78.8	−15.87	−122.1	4.9
9 Jan. 1835	0950	60.64	30.37	996	0.3	1.1	84.4	−15.45	−123.3	0.3
10 Jan. 0800	0645	63.40	32.00	998	0.7	1.2	81.2	−16.12	−124.6	4.4
Leg 2 (Antarctic Coastal Area)										
10 Jan. 1745	0840	65.10	33.75	995	−0.3	0.0	80.1	−17.17	−134.0	3.4
11 Jan. 0610	0435	65.32	34.54	994	−0.3	0.1	79.7	−17.24	−132.2	5.8
11 Jan. 1145	0200	65.46	34.55	994	−1.6	0.1	80.7	−19.27	−150.5	3.6
11 Jan. 1502	0228	65.45	34.40	994	−1.7	0.1	84.3	−21.79	−163.3	11.1
11 Jan. 1845	0152	65.44	34.34	994	−1.9	0.2	82.6	−22.32	−169.0	9.6
11 Jan. 2218	0337	65.71	35.03	994	−1.5	−0.1	76.5	−23.94	−182.8	8.7
12 Jan. 0305	0218	66.17	35.94	993	−2.1	0.2	79.7	−24.97	−187.1	12.7
12 Jan. 0710	0805	66.17	36.15	994	−1.0	0.4	78.8	−22.15	−168.1	9.0
12 Jan. 1705	1030	65.74	36.11	997	−1.3	0.4	79.5	−22.98	−170.2	13.6
13 Jan. 0652	0828	65.15	36.05	997	0.9	1.0	84.0	−16.92	−130.2	5.1
13 Jan. 1703	0857	65.12	35.32	995	0.2	0.6	94.6	−13.57	−113.6	−5.0
14 Jan. 0740	0738	65.02	37.89	992	1.4	1.6	93.4	−15.46	−126.8	−3.1
14 Jan. 1845	0901	65.33	38.00	984	0.5	1.7	96.9	−14.58	−120.1	−3.4
15 Jan. 1300	0220	66.83	37.76	971	−0.5	0.1	95.7	−17.58	−139.2	1.5
15 Jan. 1655	1013	66.82	37.71	971	−0.5	0.0	95.1	−15.87	−128.1	−1.1
16 Jan. 0655	0755	66.59	39.01	977	−0.1	0.3	95.2	−13.32	−111.5	−5.0
16 Jan. 1710	1024	66.09	40.77	981	0.0	1.5	94.4	−13.82	−113.0	−2.4
17 Jan. 0621	0829	66.01	41.11	987	0.1	1.4	87.2	−15.12	−118.7	2.3
17 Jan. 1703	1157	65.48	42.88	987	−0.2	1.2	88.6	−14.88	−115.6	3.5
18 Jan. 1452	0823	65.50	49.76	987	−0.9	−0.2	75.4	−22.24	−160.0	17.9
19 Jan. 0025	0837	65.87	51.27	991	0.4	−0.1	60.2	−23.13	−174.1	10.9
19 Jan. 1015	1657	65.34	54.97	992	0.0	0.2	70.7	−18.35	−139.1	7.7
Leg 3 (Antarctica to Fremantle)										
20 Jan. 0540	0902	64.29	61.83	991	0.4	1.0	93.5	−13.27	−108.9	−2.8
21 Jan. 0440	0515	62.39	71.16	995	0.4	1.7	85.4	−15.61	−114.9	10.0
21 Jan. 1110	0650	61.51	74.27	995	0.3	1.8	77.0	−16.41	−120.9	10.4
21 Jan. 1942	0808	60.54	77.48	994	0.0	2.1	93.3	−15.54	−115.4	9.0
22 Jan. 0515	0655	59.45	80.79	994	1.8	2.6	74.1	−17.39	−124.3	14.8
22 Jan. 1333	0522	58.61	83.47	993	1.4	2.8	74.2	−16.45	−123.5	8.1
22 Jan. 2015	0713	57.78	85.53	993	1.8	3.3	73.7	−17.49	−130.1	9.8
23 Jan. 0455	0600	56.45	88.19	995	3.6	3.5	67.3	−17.86	−131.0	11.9
23 Jan. 1215	0603	55.41	90.24	998	3.4	3.5	70.9	−16.49	−122.8	9.1
23 Jan. 1940	0650	54.53	91.82	1003	4.6	3.7	69.5	−15.95	−115.0	12.6
24 Jan. 0636	0424	53.27	93.91	1006	5.8	4.4	64.4	−15.94	−116.5	11.0
24 Jan. 1655	0805	51.89	95.97	999	4.8	5.0	86.2	−14.64	−110.0	7.1
25 Jan. 0946	0409	49.60	98.94	992	6.3	5.9	91.4	−12.27	−98.7	−0.5
25 Jan. 1515	0933	48.66	100.27	998	6.2	6.0	84.1	−13.47	−105.7	2.0
26 Jan. 0320	0755	47.19	102.15	1008	7.7	7.4	78.7	−13.96	−108.9	2.8
26 Jan. 1445	0926	45.18	104.34	1013	8.8	9.8	80.8	−13.83	−107.0	3.6
27 Jan. 0255	0415	43.56	105.98	1016	10.0	10.6	83.7	−13.52	−104.4	3.7
27 Jan. 1110	0430	42.11	107.30	1020	10.4	11.8	66.1	−15.09	−109.5	11.2
27 Jan. 1700	0630	40.76	108.35	1022	10.8	12.5	63.0	−16.13	−116.6	12.5
28 Jan. 0505	0350	38.89	110.02	1024	12.5	14.6	66.4	−15.07	−106.2	14.4
28 Jan. 1025	0430	37.99	110.99	1025	13.0	15.6	61.8	−15.69	−109.3	16.2
28 Jan. 1615	0650	36.79	112.13	1024	13.8	16.2	64.2	−15.29	−105.8	16.5
29 Jan. 0030	0430	35.55	113.05	1025	15.2	16.8	58.2	−15.46	−104.7	19.0
29 Jan. 0645	0400	34.48	113.70	1023	17.2	18.6	62.3	−14.92	−100.4	19.0
29 Jan. 1210	0455	33.47	114.35	1022	17.0	19.4	67.3	−14.60	−97.9	18.9

[a]Latitude and longtitude are shown in decimal system.

a ship funnel was passed through the bypass line. Except for this modification, the apparatus and sampling protocols are the same as described in section 2.1. The inlet air was pulled through the apparatus (flow rate, 2.0 L/min). The collected vapor sample was melted; then poured into the glass bottle and sealed with a screw cap and wrapped with Parafilm. The

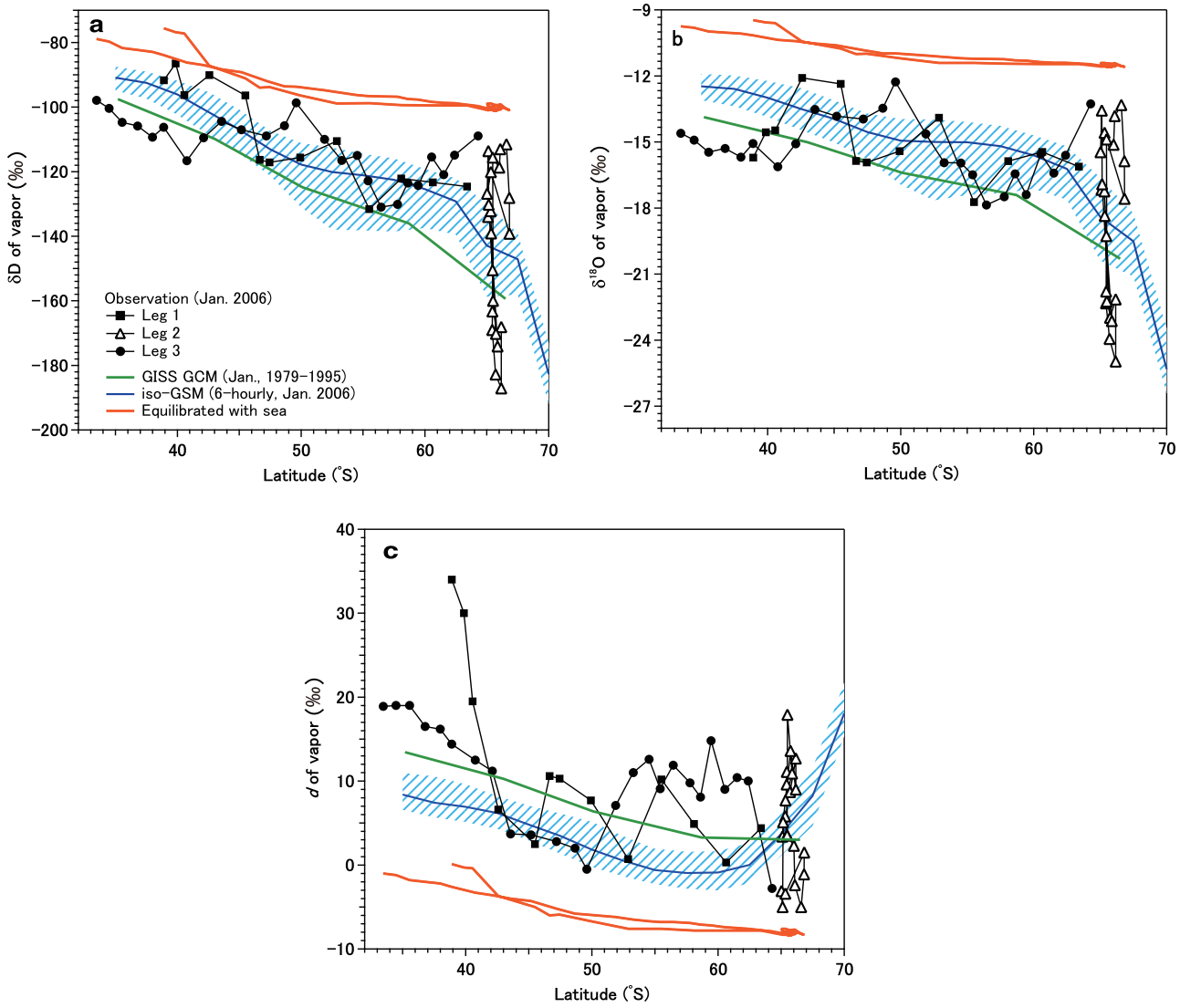

Figure 4. Latitudinal distribution of δD, δ^{18}O and d in water vapor. (a) The δD in water vapor near the ocean surface along with latitude. (b) The δ^{18}O in water vapor near the ocean surface along with latitude. (c) The d in water vapor near the ocean surface along with latitude. The observed data between 35–65°S (solid squares and circles) and south of 65°S (open triangles). The vapor isotopically equilibrated with seawater at SST is shown by the orange lines. The marine vapor δD predicted by the iso-GSM averaged value of January 2006 is shown by the blue lines. Variations of numerous model predictions are shown as 1σ (shown by the light blue shaded areas) of the latitudinal averaged value. The GISS model is shown by the green lines.

samples were transported back to the laboratory for isotope analysis.

[12] Isotope measurements of water were conducted using an isotope ratio mass spectrometer (Finnigan MAT-252 and Delta-plus; Thermo Fisher Scientific Inc., Bremen, Germany) and an automated equilibrator. The isotope compositions of 60 vapor samples were measured using an automated microequilibration technique [*Uemura et al.*, 2007]. The sample sizes used for isotope analysis were 1.0 ml (32 samples) and 0.2 ml (28 samples). The precision (1σ) of isotope measurements are 0.5‰ for δD and 0.05‰ for δ^{18}O. The observed data are shown in Table 2.

2.3. Isotope General Circulation Model

[13] To examine the daily variations of vapor change, we used high time resolution simulation results produced by the newly developed Isotope Global Spectral Model (iso-GSM) [*Yoshimura et al.*, 2008]. The iso-GSM is an isotope-incorporating version of the Global Spectral Model. The simulation shown here was performed in T62 horizontal resolution (~200 km) and 28 vertical sigma levels using the spectral nudging technique for large-scale thermodynamic features in the Reanalysis atmosphere [*Yoshimura and Kanamitsu*, 2008]. Further model details are obtainable from the literature [*Yoshimura et al.*, 2008].

3. Results and Discussions

3.1. Isotope Ratios in Vapor

[14] A backward three-dimensional trajectory for the sampled air mass was performed using the NIPR trajectory model [*Tomikawa and Sato*, 2005] with the NCEP/DOE

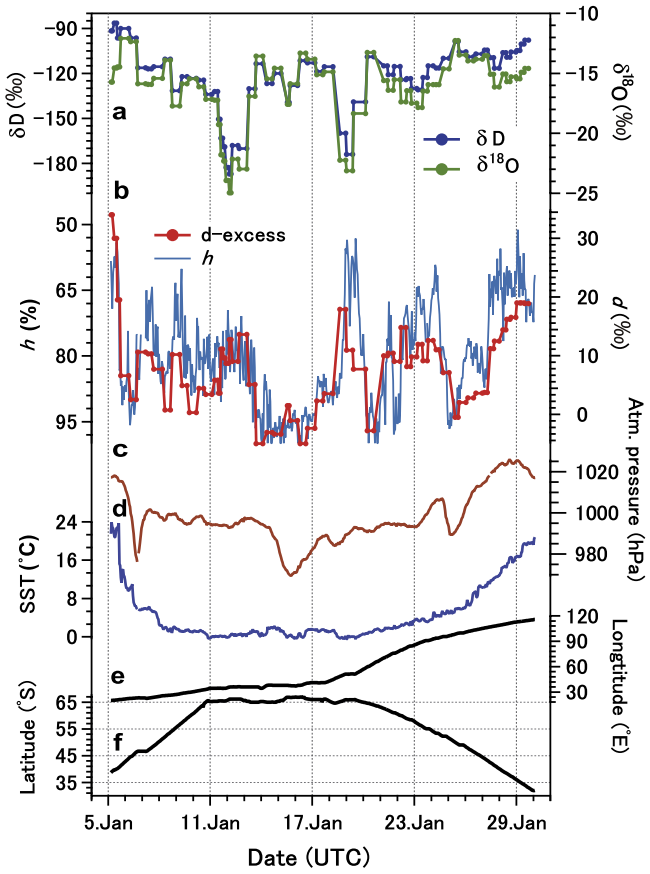

Figure 5. Time series of isotope compositions and metrological conditions. (a) Stable isotope compositions of water vapor with δD given in blue and δ^{18}O given in green. (b) Deuterium excess, d, show in red and relative humidity (h) shown in blue with an inverted axis. (c) Atmospheric pressure shown in brown. (d) Sea surface temperature given in blue. (e) The south latitude and (f) the east longitude of the *R/V* Umitaka-maru both given in black.

AMIP-II Reanalysis program of the National Centers for Environmental Prediction (NCEP)/National Center for Atmospheric Research (NCAR). A backward trajectory was released in the atmospheric boundary layer (960 hPa) over a 2 day period. The trajectory analysis suggests that the sampled air mass originated from the ocean, except for air masses near Antarctic coastal areas (Figure 1).

[15] The observed δD in vapor shows a decreasing trend, from ~−90‰ to ~−125‰ along with higher degrees of latitude from 30°S to 60°S (Figure 4a). The δD value does not reach isotopic equilibrium with seawater because of kinetic isotope effects during evaporation. Large variation of δD is found south of 65°S (Figure 4a). The time series of δD in vapor clearly depicts an anomalous decrease event in the Antarctic coastal area; the δD decreased sharply from ~−130‰ to ~−185‰ on 11 January and increased to ~−130‰ on 14 January (Figure 5). The variation of δD is comparable to the previous sparse observation between 30–65°S oceans (February and March 1995), which ranged from ~−100‰ to ~−180‰ with a sharp decrease in the 65°S area [*Schwarz et al.*, 1998]. These results suggest that the observation is representative of the mixture of oceanic and continental vapors in Antarctic coastal region. The vapor in the south 65°S is affected by the vapor from Antarctica with δD of −208‰ (averaged summer value at the Syowa Station, 69.00°S, 39.58°E, 21 m a.s.l.) [*Schwarz et al.*, 1996]. Consequently, we divided the data into two groups in the south 65°S (Leg 2, Antarctic coastal area) and the north 65°S (Leg 1, Cape Town to Antarctica and Leg 3, Antarctica to Fremantle).

[16] Although the δ^{18}O in vapor represents fundamentally similar features, the gradient of δ^{18}O from 30°S to 60°S is flat in comparison to that of δD (Figure 4b). For δ^{18}O, the kinetic fractionation is relatively more important than δD because the effect of equilibrium fractionation of δ^{18}O is about 10 times smaller than that of δD [*Jouzel and Koster*, 1996]. As a result, δ^{18}O does not vary as much with latitude (i.e., temperature). The importance of the difference between δD and δ^{18}O is shown clearly using the deuterium excess (d) parameter, which is a measure of this kinetic fractionation, in the next section.

3.2. Deuterium Excess in Vapor

[17] A striking feature of the ocean origin samples (north of 65°S) is that the d in vapor correlates negatively with h ($R^2 = 0.63$, $P < 0.001$, $n = 38$, Figure 6a) and positively with SST ($R^2 = 0.55$, $P < 0.001$, $n = 38$, Figure 6b). The d, increased by ~37‰ (−3 to 34‰) reflects a 39% (95 to 56%) decrease of h at the sampling location (~15 m above sea) and a 23.8°C (1.0° to 22.8°C) increase of the SST. The regression slopes of d versus h and SST are, respectively, −0.61‰/% and 0.85‰/°C. In order to examine how much variance can be explained, we conducted a multilinear regression analysis of d, h and SST. The variance increases up to 0.73, ($d = 0.45$ SST -0.42 h^* +37.9 with $R^2 = 0.73$). The result indicates that the 70% variance of d of vapor at ~15 m altitude above the ocean can be explained by the SST and relative humidity at this altitude.

[18] The d record in ice core is difficult to interpret because it depends on both the humidity and SST. The observation of vapor provides an intriguing example for understanding this equivocal relationship. Figure 5 depicts the smooth variation of SST, which contrasts against the erratic nature of d and h. On a timescale of a few days, the large variation of d (~20‰) can be attributed to the larger variation of h (~40%). However, along the entire meridional route, d is also controlled by the SST, which explains the smaller percentage of the variance of d. The d in marine vapor is unique in its correlation with h ($R^2 = 0.67$, $P < 0.001$, $n = 60$) over the entire period. The h does not correlate with δD ($R^2 = 0.01$, $P > 0.01$, $n = 60$) and δ^{18}O ($R^2 = 0.04$, $P > 0.01$, $n = 60$).

[19] Few other observations verify the evidence of d in vapor as an indicator of ocean surface conditions, although it is suggested by the vapor data in the Mediterranean Sea [*Gat et al.*, 2003], which is plotted on the extrapolation of regression line of this study (Figure 7). Note that Figure 7 plots d value against relative humidity normalized to saturated vapor pressure at the sea surface (h^*) because *Gat et al.* [2003] reported humidity as the h^*. The value of h^* can be approximated to h as described in section 1. During the observation period, h^* correlated with h ($h^* = 1.06\ h - 8.93$, $R^2 = 0.81$). Therefore, it does not alter the linear correlation if we adopt h instead of h^*. The linear relation

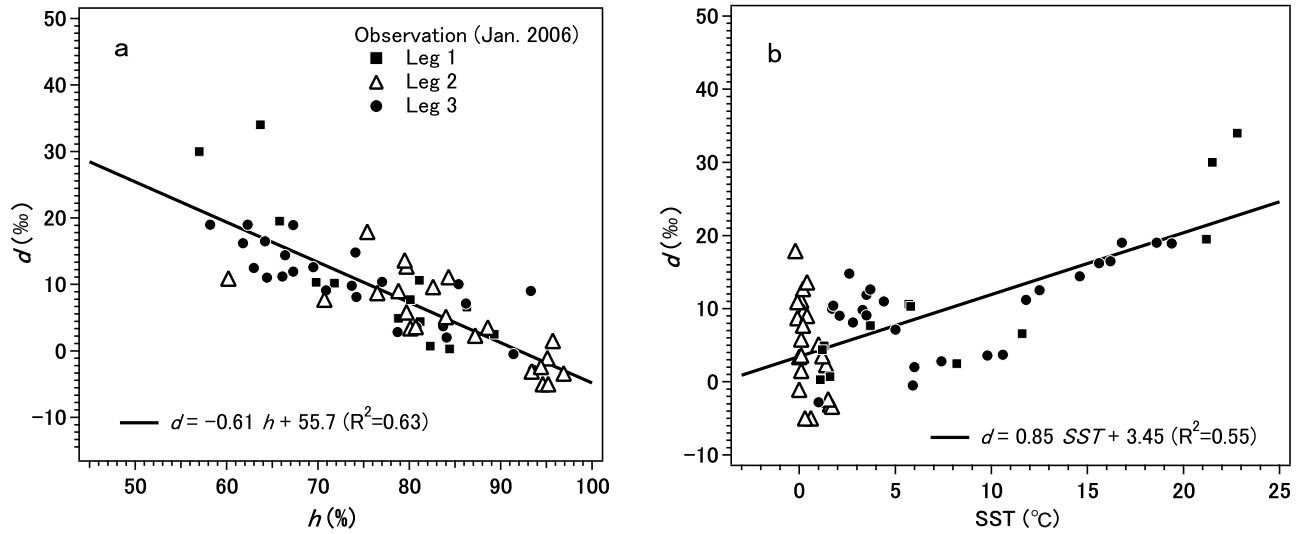

Figure 6. Correlations of d in vapor versus relative humidity and SST. (a) The d value in vapor versus relative humidity (h). (b) The d value in vapor versus SST. The observations of this study between 35°S and 65°S (Leg1 and Leg3, solid squares and circles) and south of 65°S (Leg 2, open triangles). The solid line is a linear regression line based on data observed between 35°S to 65°S (Leg1 and Leg3).

for wide range of h from the independent samplings and measurement systems strongly suggest that a physical link between the d and h^*.

[20] There is agreement between what can be predicted from equation (1) for the composition of steady state vapor, and the actual observations of the d excess. Several model results are shown in Figure 7 under typical sea-surface conditions. When we calculated the d value with equation (1) using the measured SST and humidity and plotted them against observed d, the points follow a regression line with a slope of 0.70, intersecting the y axis at −1.2‰ (d_model = 0.70* d_obs − 1.2, R^2 = 0.72). The simple model explains ~70% variance of observation. However, as discussed by [*Jouzel and Koster*, 1996], the equation (1) causes systematic bias because global-scale closure assumption ($\delta_{v0} = \delta_E$)

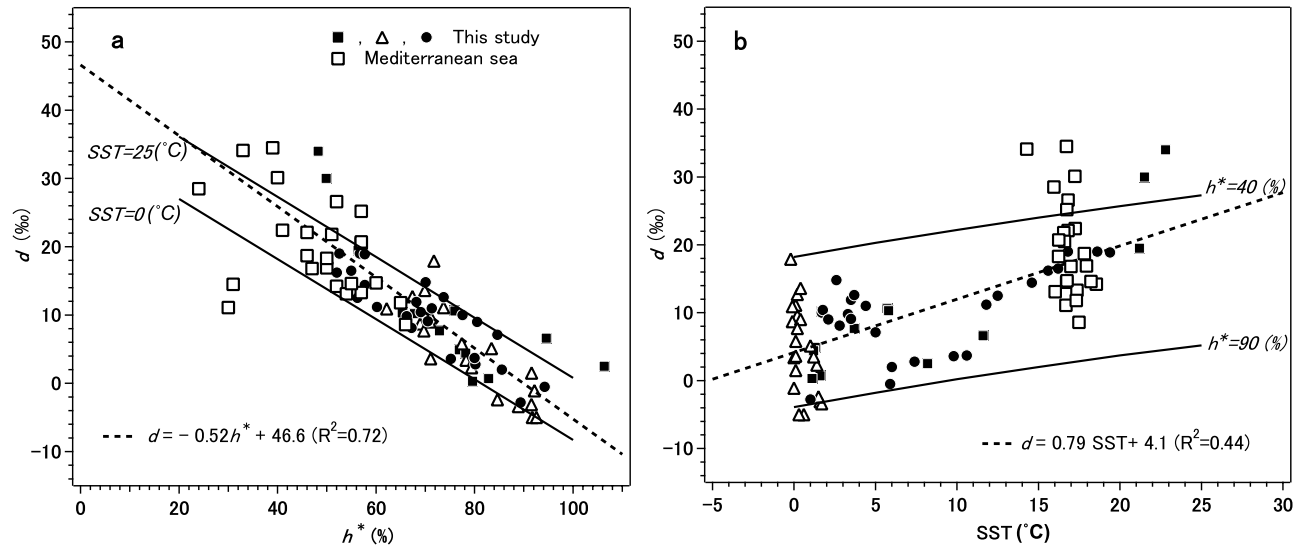

Figure 7. Comparison with simple evaporation model and observation in the Mediterranean Sea. (a) The d value in vapor versus relative humidity normalized to saturation vapor pressure at the sea surface (h^*). The observation of this study between 35 and 65°S is given by solid squares and circles and south of 65°S is given in open triangles. The dashed line represents a linear regression line based on all the data of this study. Marine vapor over the Mediterranean Sea (open squares) [*Gat et al.*, 2003]. Solid lines show the d value calculated using equation (1) [*Merlivat and Jouzel*, 1979] for different SST as marked along the solid lines. Here, we assumed smooth surface condition and used kinetic fractionation parameters, k_{18} = 6.2‰ and k_D = 5.5‰ [*Araguas-Araguas et al.*, 2000]. (b) A depiction of d versus SST. Solid lines show the d value calculated using equation (1) for different h^* as marked along the solid lines.

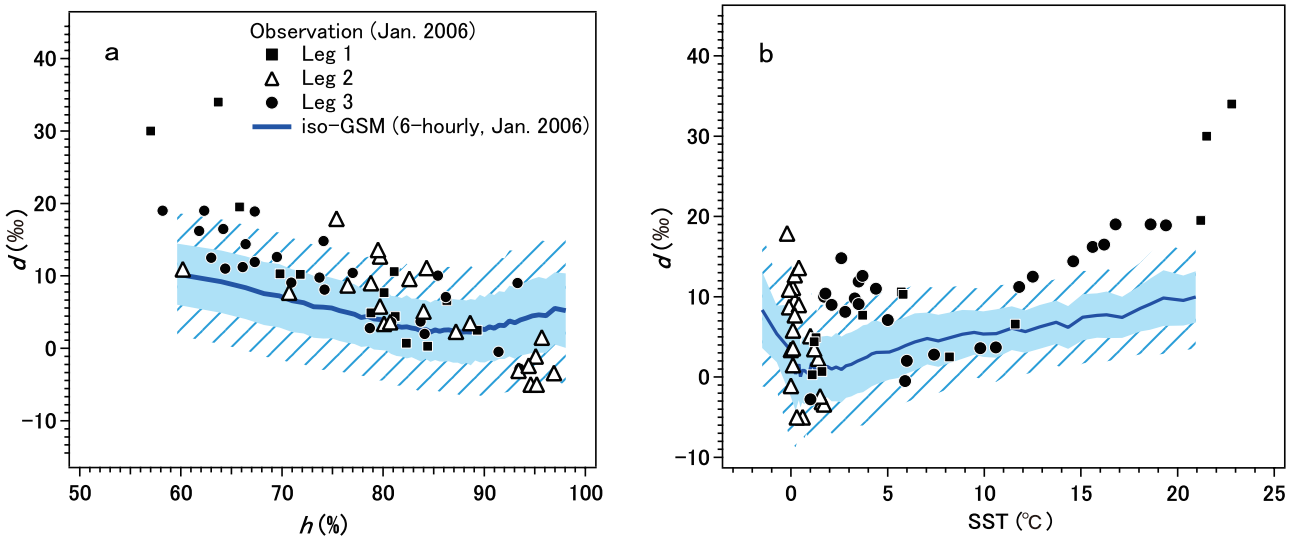

Figure 8. Comparison with GCM. Comparison with the d in marine vapor predicted by the iso-GSM averaged value of January 2006 (shown by the blue line), the standard deviations of the model predicted d, 1-sigma (shown by the blue shaded area), and 2-sigma (shown by the slashed area). (a) The d in vapor versus relative humidity (h). (b) The d in vapor versus SST.

is not valid in local scale. Therefore, we discussed further comparisons with the GCM data in the next section.

[21] A notable meteorological condition during the study is a nearby extratropical cyclone with snow around 15 January as suggested by the atmospheric pressure data in Figure 5. We observed relatively higher δD (and δ^{18}O) and lower d values during this event. An explanation of the result is that the cyclone caused high surface wind speeds and would increase sea spray. This may be an important process because the evaporation and isotopic equilibration of sea spray would lead to higher δD and lower d values. Another process is that the isotope fractionation between sea surface and atmospheric vapor is close to equilibrium state as a result of humid condition during 15 January. This simple process also leads to higher δD and lower d values. We cannot conclude the isotope effect of sea spray from the observed isotope ratios. Further observation and modeling of sea spray effect is needed.

3.3. Comparison With GCMs

[22] The isotope data of marine vapor enable examination of the validity of isotope models. Figure 4 shows the predicted ranges of variations of the isotope ratios in vapor, which are based on the ~50,000 data for the Southern Ocean (35°S–70°S and 20°E–120°E, both 2.5° steps) at 1000 hPa from 5 January to 29 January 2006 (six hourly). As climatological values, the result of the NASA Goddard Institute for Space Studies (GISS) GCM II [*Jouzel et al.*, 1987; *Delaygue et al.*, 2000] is shown (January 1979–1995, vapor in the first layer of the nine vertical layers). The ~10‰ lower δD values of the GISS model (Figure 4a) are explainable by the differences in vertical resolutions of the two models because the δD and δ^{18}O of vapor in the troposphere [*Taylor*, 1972; *Rozanski and Sonntag*, 1982; *Taylor*, 1984] decrease with altitude, ~−40‰ km^{-1} and ~−5‰ km^{-1}, respectively [*Araguas-Araguas et al.*, 2000].

[23] The δD gradient from 30°S to 60°S is consistent with the predicted January averaged variation of iso-GSM values [*Yoshimura et al.*, 2008]. The sharp decrease in δD (and δ^{18}O) observed in south of 65°S is also predicted by the iso-GSM (Figure 4a). These results confirm that the observation captures major characteristics of isotope ratios in January 2006 in spite of the short-term observation. Furthermore, the result suggests that the observed "latitude effect" of δD reflects long-term characteristics because the decreasing trend of δD is also predicted in the longer-term averaged value of the GISS GCM.

[24] The absolute value of d of iso-GSM is ~5‰ lower than the observation (See the latitude versus d plot in Figure 4c). Note that the consistency between the GISS GCM and observation would be a coincidence because the d predicted by GISS GCM reflects vapor values with altitude higher than observation and iso-GSM. Therefore, the d of GISS GCM should be lower than observation, after considering the higher d value at higher altitude. This result suggests that both the iso-GSM and GISS underestimate the d of vapor. The deficiency of d in vapor is linked directly to the fact that 2–5‰ underestimation of d in precipitation has been reported for other isotope models: ECHAM GCM [*Hoffmann et al.*, 1998] and GENESIS 2.0 GCM [*Mathieu et al.*, 2002]. Recent experimental evidence [*Cappa et al.*, 2003] suggests that, with molecular diffusivities of isotopic water molecules [*Merlivat and Jouzel*, 1979] used in most global circulation models, the d is underestimated by about 6‰. Therefore, the inclusion of the revised diffusivity ratios [*Cappa et al.*, 2003] would appear to correct the discrepancy.

[25] It is apparent that the iso-GSM shows linear relationships between d, h and SST as shown in Figure 8. Thus, the observation generally validates the relationship predicted by iso-GSM. However, the d versus h relationship disappears for h higher than about 80%. This is not the case for the observation that keeps linear trend for higher h condition. The d predicted by the iso-GSM slightly increases when h increases from 80% to 100%, and similar trend was found in GISS model [*Jouzel et al.*, 1987]. A possible cause of this discrepancy lies in description of evaporation and isotopic

exchange from liquid raindrop into unsaturated air [*Stewart*, 1975]. In fact, when we remove this process from iso-GSM, the predicted *d* value was improved (not shown here). This discrepancy should be examined further in detail.

4. Conclusions

[26] We measured the isotopic compositions of marine vapor for a wide range of ocean surface conditions. The large variation of δD and δ^{18}O found south of 65°S is attribute to the mixture of marine and Antarctic vapors. The δD in vapor decreases along with higher latitude from 30°S to 60°S. As a result of kinetic fractionation during the evaporation, latitudinal distributions of δD and δ^{18}O in vapor show slightly different behavior. The gradient of δ^{18}O from 30°S to 60°S is flat in comparison to that of δD. The observations are consistent with isotope ratios simulated by the iso-GSM, and thus validate the simulation.

[27] The *d* in vapor shows statistically significant correlations with *h* and SST. The value of these new data is that they provide the first evidence for a close relation between *d* and ocean surface conditions in different southern oceans. Regardless of the fact that the source region changes of *d* further modified during atmospheric transport [*Hendricks et al.*, 2000], precipitation, and snow formation [*Jouzel and Merlivat*, 1984], the results improve the reliability of *d* as a proxy of moisture source conditions and as a tracer of water circulation.

[28] Further observation in other oceans is needed including seasonal and vertical variation of isotope ratios in water vapor because existing data is not sufficient to calibrate the surface vapor value of isotope GCMs. Future studies must explore changes in vapor isotope contents through subsequent transportation and condensation processes occurring above the ocean and over the polar ice sheets. As shown in recent analysis of the ice core[*Landais et al.*, 2008], the addition of ^{17}O information of water (^{17}O excess) may allow decoupling of changes in the temperature of the ocean from changes in the relative humidity above it [*Angert et al.*, 2004] [*Barkan and Luz*, 2007].

[29] **Acknowledgments.** We thank the Umitaka-maru 18th cruise members, H. Kobayashi of Yamanashi Univ. and G. Hashida, T. Odate, N. Kasamatsu, and T. Hirawake of NIPR for supporting our field work and M. Yabuki of NIPR and T. Yamanaka of Tsukuba Univ. for advice on the vapor sampler. We also thank J. Jouzel and V. Masson-Delmotte of LSCE for granting access the GISS GCM data and K. Kawamura of NIPR for comments. This study was supported by a grant of JSPS Research Fellowships for Young Scientists.

References

Angert, A., C. D. Cappa, and D. J. DePaolo (2004), Kinetic ^{17}O effects in the hydrologic cycle: Indirect evidence and implications, *Geochim. Cosmochim. Acta*, *68*(17), 3487–3495, doi:10.1016/j.gca.2004.02.010.

Araguas-Araguas, L., K. Froehlich, and K. Rozanski (2000), Deuterium and oxygen-18 isotope composition of precipitation and atmospheric moisture, *Hydrol. Processes*, *14*, 1341–1355, doi:10.1002/1099-1085(20000615)14:8<1341::AID-HYP983>3.0.CO;2-Z.

Barkan, E., and B. Luz (2007), Diffusivity fractionations of $H_2^{16}O/H_2^{17}O$ and $H_2^{16}O/H_2^{18}O$ in air and their implications for isotope hydrology, *Rapid Commun. Mass Spectrom.*, *21*, 2999–3005, doi:10.1002/rcm.3180.

Cappa, C. D., M. B. Hendricks, D. J. DePaolo, and C. Cohen (2003), Isotopic fractionation of water during evaporation, *J. Geophys. Res.*, *108*(D16), 4525, doi:10.1029/2003JD003597.

Ciais, P., and J. Jouzel (1994), Deuterium and oxygen 18 in precipitation: Isotopic model, including mixed cloud process, *J. Geophys. Res.*, *99*(D8), 16,793–16,803, doi:10.1029/94JD00412.

Craig, H., and L. I. Gordon (1965), Deuterium and oxygen 18 variations in the ocean and the marine atmosphere, in *Stable Isotopes in Oceanographic Studies and Paleotemperatures*, edited by E. Tongiorgi, pp. 9–130, Lab. Geol. Nucl., Pisa, Italy.

Cuffey, K. M., and F. Vimeux (2001), Covariation of carbon dioxide and temperature from the Vosotok ice core after deuterium-excess correction, *Nature*, *412*, 523–527, doi:10.1038/35087544.

Dansgaard, W. (1964), Stable isotopes in precipitation, *Tellus*, *16*, 436–468.

Delaygue, G., V. Masson, J. Jouzel, and R. D. Koster (2000), The origin of Antarctic precipitation: A modelling approach, *Tellus Ser. B*, *52*, 19–36.

EPICA Community Members (2004), Eight glacial cycles from an Antarctic ice core, *Nature*, *429*, 623–628, doi:10.1038/nature02599.

Gat, J. R., and I. Garmi (1970), Evolution of the isotopic composition of atmospheric waters in the Mediterranean Sea area, *J. Geophys. Res.*, *75*(15), 3039–3048, doi:10.1029/JC075i015p03039.

Gat, J. R., B. Klein, Y. Kushnir, W. Roether, H. Wernli, R. Yam, and A. Shemesh (2003), Isotope composition of air moisture over the Mediterranean Sea: An index of the air-sea interaction pattern, *Tellus Ser. B*, *55*, 953–965.

He, H., and R. B. Smith (1999), An advective-diffusive isotopic evaporation-condensation model, *J. Geophys. Res.*, *104*(D15), 18,619–18,630, doi:10.1029/1999JD900335.

Hendricks, M. B., D. J. DePaolo, and R. C. Cohen (2000), Space and time variation of δ^{18}O and δD in precipitation: Can paleotemperature be estimated from ice cores?, *Global Biogeochem. Cycles*, *14*(3), 851–861, doi:10.1029/1999GB001198.

Hoffmann, G., M. Werner, and M. Heimann (1998), Water isotope module of the ECHAM atmospheric general circulation model: A study on timescales from days to several years, *J. Geophys. Res.*, *103*(D14), 16,871–16,896, doi:10.1029/98JD00423.

Horibe, Y., and Y. Takakuwa (1973), Isotope separation factor of carbon dioxide-water sysytem and isotopic composition of atmospheric oxygen, *J. Geophys. Res.*, *78*(15), 2625–2629, doi:10.1029/JC078i015p02625.

Johnsen, S. J., W. Dansgaard, and J. W. C. White (1989), The origin of Arctic precipitation under present and glacial conditions, *Tellus Ser. B*, *41*, 452–468.

Joussaume, S., R. Sadourny, and J. Jouzel (1984), A general circulation model of water isotope cycles in the atmosphere, *Nature*, *311*, 24–29, doi:10.1038/311024a0.

Jouzel, J., and R. D. Koster (1996), A reconsideration of the initial conditions used for stable water isotope models, *J. Geophys. Res.*, *101*(D17), 22,933–22,938, doi:10.1029/96JD02362.

Jouzel, J., and L. Merlivat (1984), Deuterium and oxygen 18 in precipitation: Modeling of the isotopic effects during snow formation, *J. Geophys. Res.*, *89*(D7), 11,749–11,757, doi:10.1029/JD089iD07p11749.

Jouzel, J., L. Merlivat, and C. Lorius (1982), Deuterium excess in an East Antarctic ice core suggests higher relative humidity at the oceanic surface during the last glacial maximum, *Nature*, *299*, 688–691, doi:10.1038/299688a0.

Jouzel, J., G. L. Russell, R. J. Suozzo, R. D. Koster, J. W. C. White, and W. S. Broecker (1987), Simulations of the HDO and $H_2^{18}O$ atmospheric cycyles using the NASA GISS general circulation model: The seasonal cycle for present-day conditions, *J. Geophys. Res.*, *92*(D12), 14,739–14,760, doi:10.1029/JD092iD12p14739.

Kawamura, K., et al. (2007), Northern Hemisphere forcing of climatic cycles in Antarctica over the past 360000 years, *Nature*, *448*, 912–916, doi:10.1038/nature06015.

Landais, A., E. Barkan, and B. Luz (2008), Record of δ^{18}O and ^{17}O-excess in ice from Vostok Antarctica during the last 150000 years, *Geophys. Res. Lett.*, *35*, L02709, doi:10.1029/2007GL032096.

Lawrence, J. R., S. D. Gedzelman, D. Dexheimer, H.-K. Cho, G. D. Carrie, R. Gasparini, C. R. Anderson, K. P. Bowman, and M. I. Biggerstaff (2004), Stable isotopic composition of water vapor in the tropics, *J. Geophys. Res.*, *109*, D06115, doi:10.1029/2003JD004046.

Masson-Delmotte, V., J. Jouzel, A. Landais, M. Stievenard, S. J. Johnsen, J. W. C. White, M. Werner, A. Sveinbjornsdottir, and K. Fuhrer (2005), GRIP deuterium excess reveals rapid and orbital-scale changes in Greenland moisture origin, *Science*, *309*, 118–121, doi:10.1126/science.1108575.

Mathieu, R., D. Pollard, J. E. Cole, J. W. C. White, R. S. Webb, and S. L. Thompson (2002), Simulation of stable water isotope variations by the GENESIS GCM for modern conditions, *J. Geophys. Res.*, *107*(D4), 4037, doi:10.1029/2001JD900255.

Merlivat, L., and J. Jouzel (1979), Global climatic interpretation of the deuterium-oxygen 18 relationship for precipitation, *J. Geophys. Res.*, *84*(C8), 5029–5033, doi:10.1029/JC084iC08p05029.

Noone, D. (2008), The influence of midlatitude and tropical overturning circulation on the isotopic composition of atmospheric water vapor and

Antarctic precipitation, *J. Geophys. Res.*, *113*, D04102, doi:10.1029/2007JD008892.

Rozanski, K., and C. Sonntag (1982), Vertical distribution of deuterium in atmospheric water vapour, *Tellus*, *34*, 135–141.

Schwarz, G., K. Ohm, T. Yamanouchi, T. Furukawa, P. Kowski, and H. Gernandt (1996), Stable isotopic composition of Antarctic air moisture and precipitation, *Nankyoku Shiryo*, *40*(2), 169–178.

Schwarz, G., P. Kowski, S. Kaneto, and H. Gernandt (1998), Meridional distribution of deuterium in atmospheric water vapour between tropical and southern polar latitudes, *Mem. Natl. Inst. Polar Res. Spec. Issue Jpn.*, *52*, 102–110.

Stenni, B., V. Masson-Delmotte, S. Johnsen, J. Jouzel, A. Longinelli, E. Monnin, R. Röthlisberger, and E. Selmo (2001), An oceanic cold reversal during the last deglaciation, *Science*, *293*, 2074–2077, doi:10.1126/science.1059702.

Stewart, M. K. (1975), Stable isotope fractionation due to evaporation and isotopic exchange of falling water drops, *J. Geophys. Res.*, *80*, 1138–1146.

Taylor, C. B. (1972), The vertical variations of isotopic concentrations of tropospheric water vapour over Continental Europe, and their relationship to tropospheric structure, *Rep. INS-R-107*, 45 pp., N. Z. Inst. of Nucl. Sci., Lower Hutt, New Zealand.

Taylor, C. B. (1984), Vertical distribution of deuterium in atmospheric water vapour: Problems in application to assess atmospheric condensation models, *Tellus Ser. B*, *36*, 67–72.

Tomikawa, Y., and K. Sato (2005), Design of the NIPR trajectory model, *Polar Meteorol. Glaciol.*, *19*, 120–137.

Uemura, R., N. Yoshida, N. Kurita, M. Nakawo, and O. Watanabe (2004), An observation-based method for reconstructing ocean surface changes using a 340,000-year deuterium excess record from the Dome Fuji ice core, Antarctica, *Geophys. Res. Lett.*, *31*, L13216, doi:10.1029/2004GL019954.

Uemura, R., Y. Matsui, H. Motoyama, and N. Yoshida (2007), Deuterium and oxygen-18 determination of microliter quantities of a water sample using an automated equilibrator, *Rapid Commun. Mass Spectrom.*, *21*, 1783–1790, doi:10.1002/rcm.3022.

Vimeux, F., V. Masson, J. Jouzel, M. Stievenard, and J. R. Petit (1999), Glacial-interglacial changes in ocean surface conditions in the Southern Hemisphere, *Nature*, *398*, 410–413, doi:10.1038/18860.

Vimeux, F., V. Masson, G. Delaygue, J. Jouzel, J. R. Petit, and M. Stievenard (2001), A 420,000 year deuterium excess record from East Antarctica: Information on past changes in the origin of precipitation at Vostok, *J. Geophys. Res.*, *106*(D23), 31,863–31,873, doi:10.1029/2001JD900076.

Vimeux, F., K. M. Cuffey, and J. Jouzel (2002), New insights into Southern Hemisphere temperature changes from Vostok ice cores using deuterium excess correction, *Earth Planet. Sci. Lett.*, *203*, 829–843.

Worden, J., et al. (2007), Importance of rain evaporation and continental convection in the tropical water cycle, *Nature*, *445*, 528–532, doi:10.1038/nature05508.

Yamanaka, T., and R. Shimizu (2007), Spatial distribution of deuterium in atmospheric water vapor: Diagnosing sources and the mixing of atmospheric moisture, *Geochim. Cosmochim. Acta*, *71*, 3162–3169, doi:10.1016/j.gca.2007.04.014.

Yoshimura, K., and M. Kanamitsu (2008), Dynamical global downscaling of global reanalysis, *Mon. Weather Rev.*, *136*, 2983–2998.

Yoshimura, K., M. Kanamitsu, D. Noone, and T. Oki (2008), Historical isotope simulation using reanalysis atmospheric data, *J. Geophys. Res.*, doi:10.1029/2008JD010074, in press.

Y. Matsui, School of Earth Sciences, Ohio State University, 275 Mendenhall Laboratory, 125 South Oval Mall, Columbus, OH 43210, USA.

H. Motoyama, National Institute of Polar Research, Research Organization of Information and Systems, 1-9-10 Kaga, Itabashi-ku, Tokyo 173-8515, Japan.

R. Uemura, Laboratoire des Sciences du Climat et l'Environnement, CEA-CNRS, Bat 701, L'Orme des Merisiers, F-91191 Gif-sur-Yvette, France. (ryu.uemura@lsce.ipsl.fr)

N. Yoshida, Department of Environmental Science and Technology, Tokyo Institute of Technology G1-25, 4259 Nagatsuta, Midori-ku, Yokohama 226-8502, Japan.

K. Yoshimura, Climate Research Division, Scripps Institution of Oceanography, Mail Stop 0224, La Jolla, CA 92093-0224, USA.